Available online at www.sciencedirect.com
SCIENCE DIRECT
Journal of Solid State Chemistry 179 (2006) 1093–1099
JOURNAL OF SOLID STATE CHEMISTRY
www.elsevier.com/locate/jssc

High-temperature phase equilibria in the oxide systems $SrFe_{1-x}Ga_xO_{2.5}$–$SrFe_{1-x}Ga_xO_3$ ($x = 0$, 0.1, 0.2)

I.A. Leonidov[a], M.V. Patrakeev[a], J.A. Bahteeva[a], E.B. Mitberg[a], V.L. Kozhevnikov[a,*], P. Colomban[b], K.R. Poeppelmeier[c]

[a]*Institute of Solid State Chemistry, Ural Division of RAS, #91Pervomaiskaia Str., GSP-145, 620219 Ekaterinburg, Russia*
[b]*Centre National de la Recherche Scientifique, Université Pierre et Marie Curie, Thiais, France*
[c]*Northwestern University, Department of Chemistry, 2145 Sheridan Road, Evanston, IL 60208, USA*

Received 3 October 2005; received in revised form 16 December 2005; accepted 30 December 2005
Available online 9 February 2006

Abstract

X-ray powder diffraction, Raman scattering, equilibrium oxygen content and conductivity data are combined to construct high-temperature phase diagrams (T vs. δ) for the oxide systems $SrFe_{1-x}Ga_xO_{2.5}$–$SrFe_{1-x}Ga_xO_3$, where $x = 0$, 0.1, and 0.2. Depending on oxygen content and gallium doping, three different structural types are shown to exist at high temperatures including cubic perovskite-, cubic brownmillerite-, and orthorhombic brownmillerite-type structures. Substitution of gallium for iron is shown to extend the oxygen content and temperature limits where the cubic brownmillerite-type phase is stable.

Keywords: Strontium ferrite; Conductivity; Oxygen content; Phase diagrams

1. Introduction

Strontium ferrite $SrFeO_3$ and its doped derivatives attract interest as high temperature mixed oxide ion and electron conductors because of their potential application in membrane reactors for the partial oxidation of hydrocarbons [1–5]. As with many other oxides, the ferrite may loose oxygen from the crystal lattice on heating and, when the temperature is sufficiently high, a cubic perovskite-like phase $SrFeO_{3-\delta}$ (CP) with randomized oxygen vacancies is stable even though the concentration of oxygen vacancies (δ) is quite high. However, at extremely large concentration of these vacancies, when the composition approaches the formula $SrFeO_{2.5}$, vacancy ordering results in the orthorhombic brownmillerite-like structure (OB) which is characterized by an alternation of layers of iron–oxygen octahedra and tetrahedra. The structural vacancies in the brownmillerite phase may be partially filled with oxygen ions thus resulting in the oxidation of iron and the off-stoichiometric oxide $SrFeO_{2.5+\delta}$, where $\delta \leqslant 0.05$ [6]. According to the phase diagram for the system $SrFeO_{2.5}$–$SrFeO_3$, a two-phase region (CP + OB) separates the stability fields for CP and OB structures [6,7]. However, recent in situ neutron diffraction data give evidence to another high-temperature cubic modification of the ferrite $SrFeO_{2.5}$ [8] with the elementary cell parameter of about twice that of the cubic perovskite. Following convention, this phase is called cubic brownmillerite or CB and the respective phase diagram should be modified to account for this new phase. As previously shown [8] the transition from the orthorhombic OB structure to the CB structure involves a narrow two-phase region. Overall, considering all the available literature, oxygen depletion occurs at high temperatures resulting in the transition from the cubic perovskite $SrFeO_3$ (CP) to the orthorhombic brownmillerite $SrFeO_{2.5}$ (OB) which evolves according to the sequence CP → (CP + CB) → CB → (CB + OB) → OB, where two-phase regions are shown with parentheses. Partial replacement of iron for gallium, the latter with a stable +3 oxidation state, should favor increased thermodynamic stability and influence the temperature and oxygen content limits of

*Corresponding author. Fax: +7 343 374 44 95.
E-mail address: kozhevnikov@imp.uran.ru (V.L. Kozhevnikov).

0022-4596/$ - see front matter © 2006 Elsevier Inc. All rights reserved.
doi:10.1016/j.jssc.2005.12.036

the various structural modifications. In this paper the results obtained from X-ray diffraction, Raman scattering and measurements of electrical conductivity and oxygen non-stoichiometry are used to construct the equilibrium diagrams for the complex system $SrFe_{1-x}Ga_xO_{2.5}$–$SrFe_{1-x}Ga_xO_3$ ($x = 0$, 0.1, and 0.2) at high temperatures.

2. Experimental

The samples used in this study were prepared by solid-state reactions. Starting materials were oxides Fe_2O_3 (99.92%), Ga_2O_3 (99.99%) and strontium carbonate $SrCO_3$ (99.94%). The raw materials were weighed in desirable amounts and thoroughly mixed with a mortar and pestle with addition of ethanol. The mixtures were pressed into pellets and fired at 900–1250 °C in air. The materials were crushed into powder, pressed and fired several times with a gradual increase in temperature before single-phase specimens were obtained. Phase purity and determination of the lattice parameters were carried out with X-ray powder diffraction ($\lambda = 1.54178$ Å). The lattice parameters were refined with the using of FullProf program [9]. A part of the synthesized materials was ball-milled in ethanol media and pressed into discs under 2 kbar uniaxial load. The disks were sintered in air at 1250 °C for 10 h to a density no less than 90% of theoretical. Rectangular bars $2 \times 2 \times 18$ mm were cut from the sintered discs for the conductivity measurements.

Raman spectra were recorded directly on sample surfaces. The 458 nm line from a ArKr laser and the 532 nm line from a cw frequency doubled Nd:YAG laser were used as excitation sources. The excitation power was kept at 0.1–0.5 mW (measured on the sample) in order to avoid any thermal effects. The laser spot diameter was between 1.5 and 5 μm for the micro-Raman measurements. Raman spectrometers were a *XY* (Dilor) and a Infinity (Jobin–Yvon–Horiba). They included a back-illuminated Spex CCD 2D matrix for signal detection. The CCD was cooled either by liquid nitrogen (*XY*) or by Peltier-effect (Infinity). The spectral resolution of the *XY* and Infinity spectrometers was approximately 0.5 and 2 cm^{-1}, respectively. Plasma lines were used as reference to improve the wavenumber accuracy. The positions of the peaks in the spectra were determined by fitting the "narrow" peak with a Lorentzian [10] and the "broad" one with a Gaussian [11].

The oxygen stoichiometry in as-prepared samples was determined by iodometric titration. The equilibrium oxygen content in the samples at different values of temperature (T) and partial pressure of oxygen (pO_2) in the gaseous phase was measured by coulometric titration as described elsewhere [12]. The absolute changes of oxygen content in the specimens on heating in air ($pO_2 = 0.21$ atm) were determined with a Setaram TG-DTA-92 thermoanalyzer and combined with the iodometric titration data. The experimental uncertainties in determination of δ by coulometric titration, TG reduction and iodometric titration did not exceed 0.001, 0.005, and 0.01, respectively. The oxygen content in samples at $T = 700$ °C and $pO_2 = 0.21$ atm was used as a reference point for the coulometric titration data. Perfect matches of the TG and coulometric titration results, at the same $pO_2 = 0.21$ atm but at various temperatures, confirmed the reliability of the non-stoichiometry values (δ) obtained by coulometric measurements over the entire range of the oxygen pressure and temperature studied.

Electrical conductivity (σ) data were obtained in 4-probe d.c. experiments with the use of Pt wire potential probes and current leads. The wired specimen was sealed under an atmosphere of 50%O_2 and 50%CO_2 in the measuring cell constructed from stabilized cubic-zirconia. The cell was equipped with two pairs of Pt electrodes. One pair was used as an oxygen pump to change and maintain oxygen partial pressure, while the other was utilized as oxygen sensor in order to control independently the pO_2 inside the cell. The assembly was set in the isothermal zone of a tubular furnace where the temperature of the experiment was maintained. The electrical parameters were measured with a high-precision voltmeter Solartron 7081. Computer controlled operation of the oxygen pump and sensor provided precise variation and maintenance of the partial oxygen pressure in the cell. The measurements were carried out in the mode of decreasing oxygen partial pressure in isothermal runs.

3. Results and discussion

3.1. Sample characterization

The tetragonal elementary cell parameters in the ferrite $SrFeO_{3-\delta}$ ($x = 0$) were to $a = 10.936(2)$ and $c = 7.709(5)$ Å in good agreement with literature values [7,13]. The X-ray powder diffraction patterns for the as-prepared $SrFeO_{1-x}Ga_xO_{3-\delta}$ ($x = 0.1$ and 0.2) samples show formation of perovskite-like phases with a rhombohedral structure, see Fig. 1. The unit cell parameters and oxygen contents of the obtained samples are summarized in Table 1. The oxygen contents of the air-synthesized gallium containing specimens decrease with the introduction of gallium giving evidence to the replacement of tetravalent iron for trivalent gallium in the structure. At the same time, these changes are not very large, and the oxygen content always remains essentially close to that in the ferrite $SrFeO_{2.75}$ ($Sr_4Fe_4O_{11}$). Although substitution of gallium for iron does not result in a fundamental structural change of the perovskite-like framework of $SrFeO_{2.75}$ [13], gallium cations are known to have a strong preference for tetrahedral coordination and we speculate that the reason the doped samples $SrFe_{1-x}Ga_xO_{3-\delta}$ acquire a rhombohedral structure is that the linkage of the structural $FeO_{6/2}$ and $FeO_{5/2}$ polyhedra is evidently strongly disturbed by incorporation of these $GaO_{4/2}$ tetrahedra.

Annealing in a reducing atmosphere (5%H_2:95%He) at 700 °C results in a loss of oxygen and formation of the

brownmillerite-like structure in all the samples, Fig. 2. The respective X-ray powder diffraction patterns of these compositions can be indexed with orthorhombic symmetry. The elementary unit cell parameters are found equal to $a_0 \approx \sqrt{2}a_p$, $b_0 \approx 4a_p$ and $c_0 \approx \sqrt{2}a_p$, where $a_p \approx 3.9$ Å (Table 1).

Raman spectra obtained with the excitation line 458 nm for the reduced, brownmillerite-like specimens are shown in Fig. 3a. The structural differences of non-doped (sample #1), Ga-substituted oxygen deficient (samples #2, 3 and 4) and oxygen-rich (samples #5 and 6) ferrites are evidenced by the change in the number of bands (from 4 to 1) and wavenumber shifts (up to $\sim 40\,cm^{-1}$). The compounds exhibiting broader Raman spectrum with smaller number of bands correspond to a higher symmetry (no Raman bands are expected for a cubic perovskite) and, thus, it is obvious that samples #5 and #6 correspond to a slightly distorted cubic phase, which is in accord with X-ray data. Samples #1 and #2 have similar number of bands though a wavenumber shift is clearly observed. The spectrum for orthorhombic $SrFeO_{2.5}$ exhibits a strong peak at $620\,cm^{-1}$ characteristic for stretching modes of relatively long bonds (1.94–2.22 Å [8]) in $FeO_{6/2}$ octahedra, while the shoulder at about $700\,cm^{-1}$ is related to vibrations of shorter bonds in $FeO_{4/2}$ tetrahedra. Replacement of iron for heavier gallium results in appearance of an intense peak at $666\,cm^{-1}$. This change cannot be explained simply based on changes in the length of Fe–O bonds because structural parameters do not vary greatly with the doping. Rather it should be attributed to Fe–O bonding changes owing to incorporation of $GaO_{4/2}$ tetrahedra in the structure. Also, considering the ionic radii for tetrahedral Fe^{3+}_{IV} (0.49 Å) and Ga^{3+}_{IV} (0.47 Å) [14], one can suppose near equality in the length of iron– and gallium–oxygen bonds which in combination with larger mass of gallium may explain the shift of the peaks at 430 and $330\,cm^{-1}$ with incorporation of gallium to 375 and $290\,cm^{-1}$, respectively. The spectra recorded with the longer wavelength, Fig. 3b, resemble those in Fig. 3a. The wavenumber shift can be seen when spectra excited with blue and green laser lines are compared. This is indicative of a strong electronic absorption in green ($\sim$2.3 eV) to blue ($\sim$2.7 eV) domains (samples are black). Consequently, the in-depth penetration of the laser light depends on the excitation wavelength, and near-resonance Raman scattering occurs. From the intensity of observed

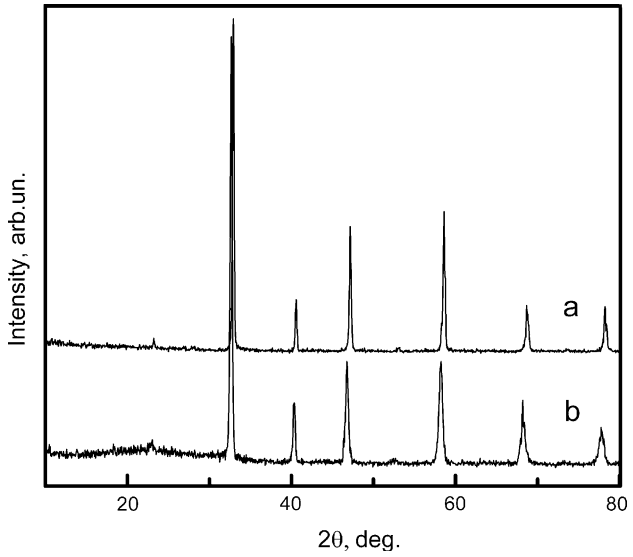

Fig. 1. X-ray powder diffraction patterns for the air-synthesized samples $SrFe_{1-x}Ga_xO_{3-\delta}$: (a) $x = 0.1$, (b) $x = 0.2$.

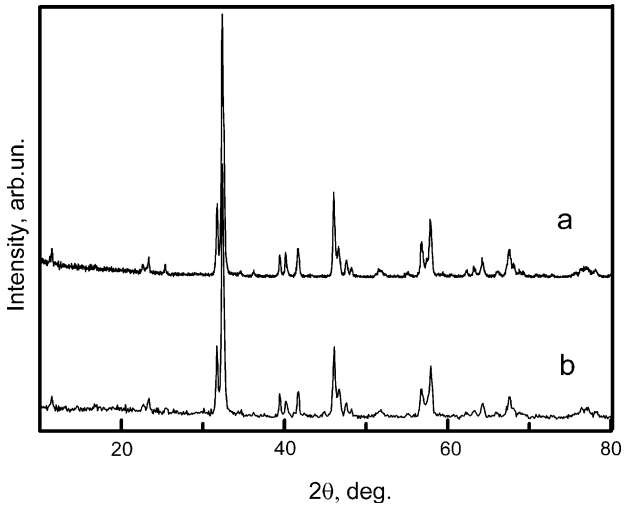

Fig. 2. X-ray powder diffractcion patterns for brownmillerite-like samples $SrFe_{1-x}Ga_xO_{2.5}$: (a) $x = 0.1$, (b) $x = 0.2$.

Table 1
The elementary unit parameters and oxygen content ($3-\delta$) in the samples of $SrFe_{1-x}Ga_xO_{3-\delta}$ obtained at synthesis in air and after heat treatment at 700 °C in 5% H_2/95% He gas mixture

Atmosphere	x	Symmetry	a (Å)	b (Å)	c (Å)	$3-\delta$
Air	0.0	Tetragonal	10.936 (2)		7.709 (5)	2.86
	0.1	Rhombohedral[a]	5.431 (6)		13.523 (6)	2.79
	0.2	Rhombohedral[a]	5.439 (2)		13.524 (0)	2.74
5% H_2/95% He	0.0	Orthorhombic	5.668 (5)	15.582 (3)	5.526 (5)	2.50
	0.1	Orthorhombic	5.647 (9)	15.561 (1)	5.510 (4)	2.50
	0.2	Orthorhombic	5.646 (1)	15.553 (6)	5.505 (7)	2.50

[a]Hexagonal setting.

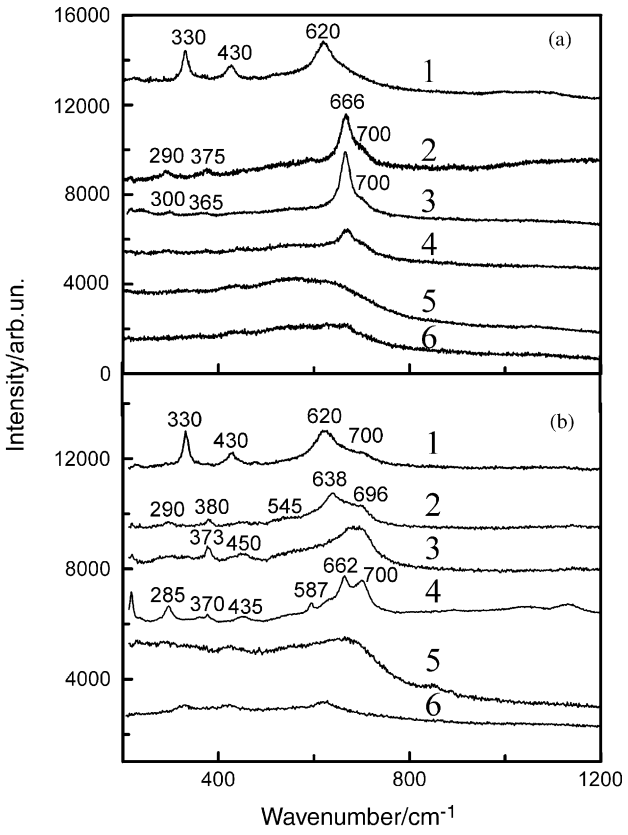

Fig. 3. Raman spectra for $SrFe_{1-x}Ga_xO_{3-\delta}$. The wavelength/laser beam power correspond to (a) 458 nm/1 mW and (b) 532 nm/0.06–0.6 mW (the excitation of spectra with the 532 nm line reveals that a (pre)resonance occurs that modifies the relative intensity of different peaks). 1—$SrFeO_{2.5}$, 2—$SrFe_{0.9}Ga_{0.1}O_{2.55}$, 3—$SrFe_{0.8}Ga_{0.2}O_{2.55}$, 4—$SrFe_{0.8}Ga_{0.2}O_{2.5}$, 5—$SrFe_{0.9}Ga_{0.1}O_{2.79}$, 6—$SrFe_{0.8}Ga_{0.2}O_{2.74}$.

harmonics we think that the near-resonance is more effective with green excitation and hence the recorded spectra highlight the surface layers of the materials. The peak detected at 638 cm^{-1} in the spectrum of $SrFe_{0.9}Ga_{0.1}O_{2.55}$ may possibly originate from stretching modes of the structural octahedra containing Fe^{4+} cations because smaller size and larger cation charge both result in shorter metal–oxygen bond lengths and, thus, in larger frequency of the vibration. The progressive transformation of orthorhombic brownmillerite to rhombohedral perovskite with the increase in amount of oxygen vacancies is supported by the Raman spectra. The broadening of the spectral lines shows that the symmetry change is associated with a strong disordering on the local scale [15]. Because Raman scattering arises from the bond polarizability change when oxygen atom moves with respect to the atom at the center of the vibrational entity ($MO_{6/2}$ octahedron or $MO_{4/2}$ tetrahedron), the bandwidth increases drastically when the number of oxygen vacancies increases and/or when the M cation valence is decreased. Thus, the large number of oxygen vacancies results in a strong disorder of the oxygen sublattice (very broad Raman spectra). The cubic or near cubic structure with a high concentration of oxygen vacancies is possibly stabilized by the long-range Coulomb interactions.

3.2. High-temperature phase diagram for the system $SrFeO_3$–$SrFeO_{2.5}$

Electrical conductivity and oxygen content data are combined [16] to plot the isothermal dependencies of conductivity vs. oxygen content in $SrFeO_{3-\delta}$, see Fig. 4. The oxygen ion conductivity in the ferrite is about 0.1 S/cm [5] or about 1% of the total conductivity. Thus, the isotherms in Fig. 4 mainly reflect behavior of the electron (hole type) conductivity. The start of the transition from cubic perovskite (CP) to orthorhombic brownmillerite phase (OB) is clearly visible in the graphs of isothermal conductivity vs. oxygen content. This rapid decrease in conductivity occurs because hole conductivity in the brownmillerite phase is considerably smaller than in the perovskite phase. The stability limits of the perovskite phase (CP) are approximately (see Fig. 4) $3-\delta \approx 2.59$ and 2.56 at 650 and 700 °C, respectively, in excellent agreement with previous results [7]. The rapid decrease in conductivity in the 650 °C isotherm is replaced by smoother changes at $3-\delta \approx 2.55$ when the ferrite adopts the brownmillerite-like structure (OB). The limiting oxygen content ($3-\delta$) of 2.55 of the brownmillerite phase (OB) at 650 °C is in agreement with earlier data reported at 600 and 700 °C [6]. Overall, previous data [6,7] and our results show that the broad non-stoichiometric oxygen range of the perovskite-like phase enlarges while the homogeneity range of the brownmillerite-like phase becomes smaller with the temperature increase. Thus the two-phase field (CP + OB) becomes rather narrow at temperatures above 700 °C, Fig. 5. This particular behavior makes it difficult to track the stability borders of these different phases at temperatures above 700 °C from the conductivity data alone. As an alternative, we implemented the coulometric titration technique in order to identify phase transitions in

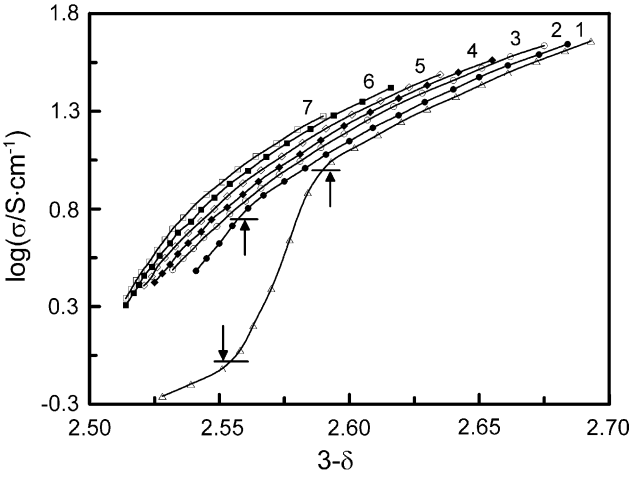

Fig. 4. The plots of electrical conductivity vs. oxygen content in $SrFeO_{3-\delta}$. The temperature of the isotherms 1, 2, 3, 4, 5, 6, and 7 corresponds to 650, 700, 750, 800, 850, 900, and 950 °C, respectively.

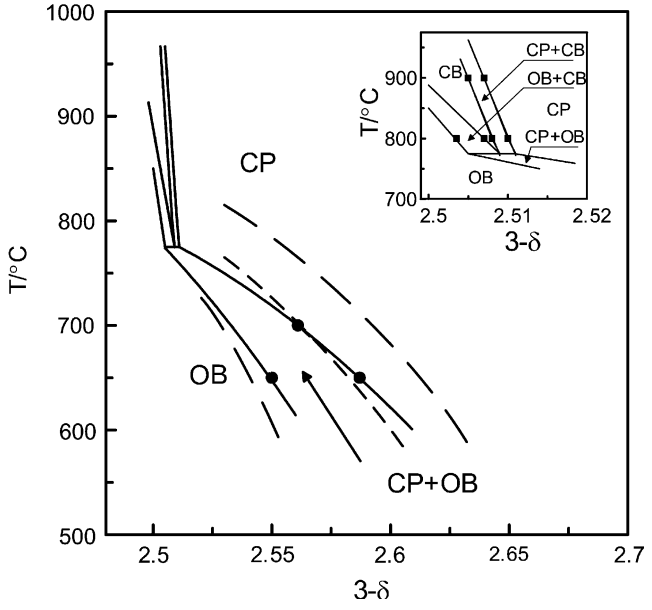

Fig. 5. The high-temperature phase diagram for $SrFeO_{3-\delta}$. The main field is constructed from electrical conductivity data (circles). The inset shows the part of the diagram above the invariant equilibrium as obtained from coulometric titration (squares). Solid lines show phase borders according to the experimental data in the present work. The short-dashed line shows the stability border of the cubic perovskite phase CP according to Ref. [7]. The long-dashed lines represent the two-phase region according to Ref. [6].

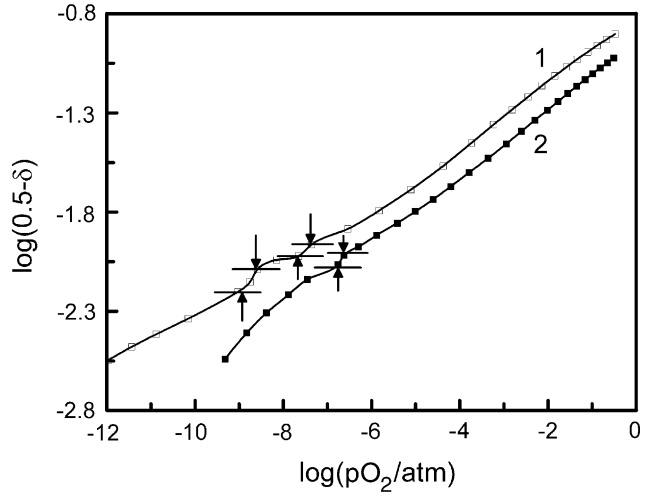

Fig. 6. The logarithmic plots of oxygen non-stoichiometry vs. oxygen partial pressure for $SrFeO_{3-\delta}$ at (1) 800, and (2) 900 °C. Up- and down-head arrows indicate pressure intervals for two-phase regions.

$SrFeO_{3-\delta}$ at higher temperatures. The respective data are presented in Fig. 6 where in order to show more clearly the difference in position of characteristic points on the measured isotherms we use parameter $(0.5-\delta)$ in place of the total oxygen content $(3-\delta)$. Two step-like features on the isotherm at 800 °C in Fig. 6 are identified as corresponding to the two-phase regions (CP + CB) and (CB + OB). In contrast, the isotherm at 900 °C reveals one two-phase region (CP + CB). A summary combining all these results and available literature data is given in Fig. 5 in the form of a generalized phase diagram where approximate positions of all phase boundaries as a function of temperature and oxygen content are indicated. The inset shows in more detail that portion of the diagram above 700 °C. Note that the composition (homogeneous oxygen range) of the CB $SrFeO_{2.5+\delta}$ phase appears to achieve a value for δ of about 0.05 at 900 °C. Also note that the temperature of the invariant equilibrium point is approximately or close to 780 °C.

3.3. High-temperature phase diagrams for the system $SrFe_{1-x}Ga_xO_{2.5}$–$SrFe_{1-x}Ga_xO_3$ (x =0.1 and 0.2)

The concentration behavior of the logarithm of the conductivity vs. oxygen content is shown in Fig. 7 for the two specimens $SrFe_{1-x}Ga_xO_{3-\delta}$; $x = 0.1$ and 0.2. The cusps on the isotherms, which are shown with arrows, identify the two-phase (OB + CP) regions. These data were used to construct the equilibrium temperature vs. oxygen content diagrams shown in Fig. 8. Compared to the all iron system the homogeneous range of the OB phase is markedly wider in the doped samples than in the parent ferrite. The cusp near $\delta \approx 0.45$ on the conductivity isotherm for $SrFe_{0.8}Ga_{0.2}O_{3-\delta}$ at 950 °C is related to the phase equilibrium CP ↔ CB. As before, conductivity measurements

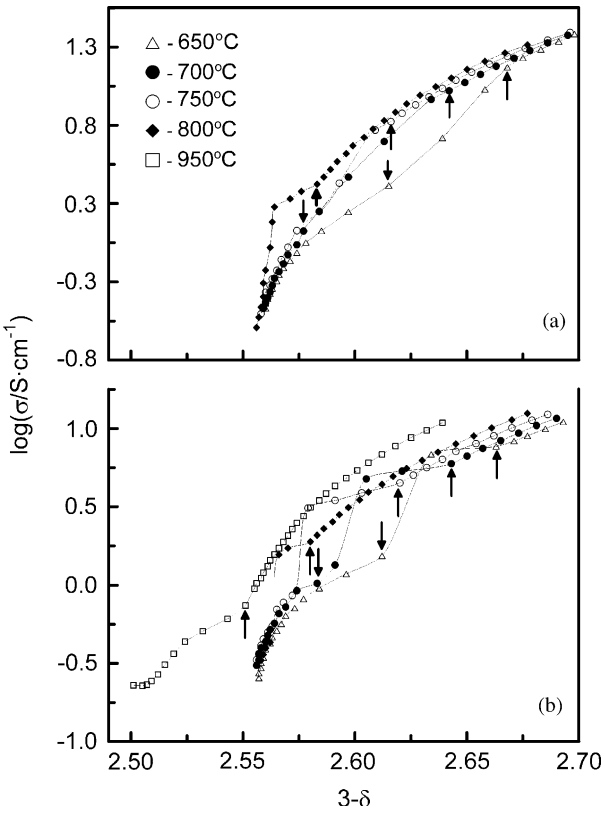

Fig. 7. The plots of electrical conductivity vs. oxygen content in $SrFe_{1-x}Ga_xO_{3-\delta}$ at (a) $x = 0.1$, and (b) $x = 0.2$. The up/down-head arrows show minimal/maximal oxygen content in the perovskite/brownmillerite phase at different temperatures.

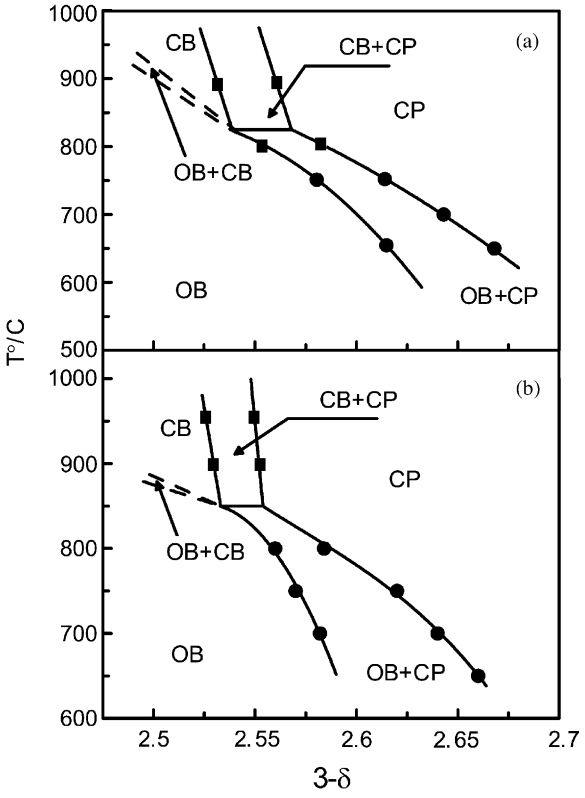

Fig. 8. The high-temperature phase diagrams for $SrFe_{1-x}Ga_xO_{3-\delta}$ at (a) $x = 0.1$, (b) $x = 0.2$. Solid lines show phase borders according to the experimental data in the present work; circles are obtained from conductivity measurements, squares represent coulometric titration data. The dashed lines tentatively delineate the two-phase (OB + CB) region.

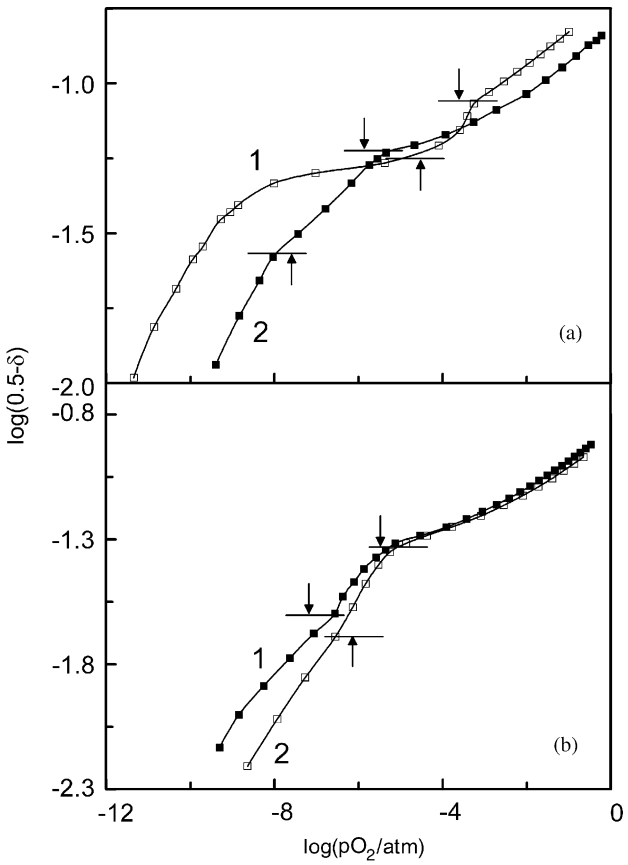

Fig. 9. The logarithmic plots of oxygen non-stoichiometry vs. oxygen partial pressure for $SrFe_{1-x}Ga_xO_{3-\delta}$, $x = 0.1$ at 800 (1) and 900 °C (a) and $x = 0.2$ at 900 (1) and 950 °C (b). Up- and down-head arrows indicate pressure intervals for the two-phase regions.

were complemented with coulometric titration data, see Fig. 9. The step-like feature on the titration isotherm for $SrFe_{0.9}Ga_{0.1}O_{3-\delta}$ at 800 °C appears because of the equilibrium CP↔OB, and the respective two-phase (OB + CP) region occurs in excellent correspondence with the results from electrical conductivity measurements at lower temperatures. The less distinct change in δ at 900 °C is due to the equilibrium CP↔CB. Similar peculiarities are seen on the isotherms $\log(\delta)-\log(pO_2)$ for $SrFe_{0.8}Ga_{0.2}O_{3-\delta}$ at 900 and 950 °C, see Fig. 9b. The two-phase (OB + CB) region is probably so narrow in the doped samples that it can not be seen on the plots $\log(\delta)$–$\log(pO_2)$. Therefore, the approximate temperatures of the phase transition OB→CB for oxides $SrFe_{1-x}Ga_xO_{2.5}$ were determined from the Arrhenius plots for the oxygen ion (σ_i) conductivity. Based on our earlier data [17], the transition in question results in a change of the slope of the plots $\log(\sigma_i)$ vs. $1/T$ and, hence, the transition temperature is at 900 and 875 °C for $SrFe_{1-x}Ga_xO_{3-\delta}$ with $x = 0.1$ and 0.2, respectively. The tentative borders for the (OB + CB) two-phase region are shown by dashed lines in Figs. 9a and b. As seen from these diagrams, the stability border of the perovskite-like CP phase does not vary substantially with the increase in gallium concentration. The single phase OB field is observed to be wider in the oxide $x = 0.1$ than in $x = 0.2$ and the temperature of the invariant equilibrium tends to increase with gallium amount. Thus, partial replacement of iron with gallium favors greater stability of the cubic CB phase and expands the region of oxygen content and temperature where it is stable compared to the all iron system.

4. Conclusions

The partial replacement of iron with gallium in perovskite-like strontium ferrite when synthesized in air ($pO_2 = 0.21$ atm) results in a substantial oxygen loss from the crystalline lattice and a strong distortion of the $FeO_{6/2}$ octahedra. Treatment in a reducing atmosphere ($pO_2 \leqslant 10^{-5}$ atm) results in formation of a brownmillerite-type structure in the oxides $SrFe_{1-x}Ga_xO_{3-\delta}$ ($x = 0$, 0.1, and 0.2) and depending on gallium doping and oxygen content the brownmillerite-type structure may be either orthorhombic (OB) or cubic (CB). X-ray diffraction, TG measurements of oxygen content and Raman spectroscopy are consistent with primarily tetrahedral coordination of the gallium dopant in the brownmillerite-type phase. The combined data from conductivity and coulometric titration measurements were used to construct high-temperature equilibrium phase diagrams as a function of temperature

and oxygen content and to delineate the phase boundaries limiting single-phase and two-phase regions. Introduction of gallium on the iron sub-lattice increased the stability of the cubic brownmillerite-type phase (CB) with respect to variations of temperature and oxygen content.

Acknowledgments

This work was partially supported by the program "Fundamental studies" (RAS #4-K-4), by the NATO SfP foundation (Grant #978002), and by the Chemical Sciences, Geosciences and Biosciences Division, Office of Basic Energy Sciences, Office of Science, US Department of Energy under Award #DE-FG02-03-ER15457.

References

[1] Y. Teraoka, H.M. Zhang, S. Furukawa, N. Yamazoe, Chem. Lett. 7 (1988) 1084–1089.
[2] J.E. ten Elshof, H.J. Bouwmeester, H. Verweij, Solid State Ionics 89 (1996) 81–92.
[3] M. Schwartz, J. White, A. Sammels, Int. Patent Appl. PCT/US96/14841, WO 97/41060 (1997).
[4] A. Holt, T. Norby, R. Glenne, Ionics 5 (1999) 434–443.
[5] V.L. Kozhevnikov, I.A. Leonidov, M.V. Patrakeev, E.B. Mitberg, K.R. Poeppelmeier, J. Solid State Chem. 158 (2001) 320–326.
[6] J. Mizusaki, M. Okaysu, S. Yamauchi, F. Fueki, J. Solid State Chem. 99 (1992) 166–172.
[7] Y. Takeda, K. Kanno, T. Takeda, O. Yamamoto, M. Takano, N. Nakayama, Y. Bando, J. Solid State Chem. 63 (1986) 237–249.
[8] M. Schmidt, S.J. Campbell, J. Solid State Chem. 156 (2001) 292–304.
[9] R. Carvajal, Physica B 192 (1993) 55–69.
[10] M. Havel, D. Baron, Ph. Colomban, J. Mater. Sci. 39 (2004) 6183–6189.
[11] P. Colomban, O. Paulse, J. Am. Ceram. Soc. 88 (2005) 390–395.
[12] M.V. Patrakeev, E.B. Mitberg, A.A. Lakhtin, I.A. Leonidov, V.L. Kozhevnikov, K.R. Poeppelmeier, Ionics 4 (1998) 191–199.
[13] J.P. Hodges, S. Short, J.D. Jorgensen, X. Xiong, B. Dabrowski, S.M. Mini, C.W. Kimball, J. Solid State Chem. 151 (2000) 1 90–209.
[14] R.D. Shannon, Acta Crystallogr. A 32 (1976) 751–754.
[15] A.I. Rykov, K. Nomura, T. Mitsui, M. Seto, Physica B 350 (2004) 287–293.
[16] M.V. Patrakeev, J.A. Shilova, E.B. Mitberg, A.A. Lakhtin, I.A. Leonidov, V.L. Kozhevnikov, in: C. Julien, et al. (Eds.), New Trends in Intercalation Compounds for Energy Storage, Kluwer Academic Publishers, Dordrecht, 2002, pp. 567–572.
[17] M.V. Patrakeev, V.L. Kozhevnikov, I.A. Leonidov, J.A. Bahteeva, E.B. Mitberg, in: N. Orlovskaya, N. Browning (Eds.), Mixed Ionic Electronic Conducting for Advanced Energy System, Kluwer Academic Publishers, Dordrecht, 2004, pp. 163–168.